Phase-field model of island growth in epitaxy

Yan-Mei Yu and Bang-Gui Liu
Institute of Physics & Center of Condensed Matter Physics, Chinese Academy of Science, P. O. Box 603, 100080 Beijing, People's Republic of China
(Received 31 August 2003; published 23 February 2004)

Nucleation and growth of islands in epitaxy is simulated using a continuum phase-field model. In addition to local density of adatoms, a local phase-field variable, varying in the real space, is introduced to describe the epitaxial islands. Evolution of this phase field is determined by a time-dependent Ginzburg-Landau-like equation coupled to a diffusive transport equation of adatoms. When applied to nucleation and growth of islands in the submonolayer regime, this model reproduces both the scaling laws of island density and experimental size and spatial distributions of islands. For island growth in the multilayer regime, this phase-field model reproduces mound structures consistent with experimental images concerned. Accurate coarsening and roughening exponents of the mounds are obtained in this model. Compared with atomic models and mean-field models, this model can provide a fine visualized morphology of islands at large space and time scales of practical engineering interests.

DOI: 10.1103/PhysRevE.69.021601 PACS number(s): 81.15.Aa, 81.10.Aj, 68.35.Ct

I. INTRODUCTION

Modeling and simulation of the island growth in epitaxy provide an effective tool to understand and manipulate epitaxial processes. Atomic models, such as kinetic Monte Carlo (KMC) simulation, allow easy implementation of a wide range of atomistic kinetic processes, and is therefore valuable in understanding microscopic mechanisms during epitaxial growth. However, it is not computationally efficient enough to describe growth on a large scale and, especially, at macroscopic scales. On the other hand, analytic mean-field models, such as rate equation, can describe the island growth of various sizes, but cannot contain any local spatial information. Therefore, it is an important task to develop a new approach that can simulate the island growth at the larger time and space scales of practical engineering interests, and at the same time contain enough local spatial information.

As is well known, epitaxial growth is based on motion of island boundaries, such as creation, aggregation, and coalescence, which is analogical in principle with the growth of steps on crystal surfaces. The well known Burton-Cabrera-Frank (BCF) model of step kinetics [1] can be extended to the island growth by treating island boundaries as steps. In this way, the movement of island boundaries is described by a diffusionlike equation of the density of adatoms subject to appropriate boundary conditions which reflect the relevant microscopic details of atomic processes on edges of the islands. The continuum formulation can make the simulation of the island growth extend to a larger spatial scale (even up to micrometers) and temporal scale (hours), but direct numerical resolution is hindered by the need to track explicitly all moving boundaries. The difficulty can be partly overcome by front tracking techniques. A level-set method was designed to use this technique to simulate the island growth, but was limited to the submonolayer regime or layer-by-layer growth because of its difficulty in treating numerical implementation and complex boundary conditions [2,3].

The phase-field method is a popular front tracking technique that is applied widely to a general category of free boundary problems known as Stefan problems, such as solidification [4], solid-solid phase transitions [5], Ostwald ripening [6], and nucleation [7]. Based on the Ginzburg-Landau theory of phase transitions, the phase-field method formulates the free boundary problem as a set of partial differential equations (PDEs) of physically relevant variables such as phase fields, concentration, density, magnetization, etc. Boundary conditions are incorporated implicitly to these equations so that tracking boundaries is avoided. At the same time, the dependence of computational results on model parameters has been greatly reduced by the *thin-interface analysis* [8]. Hence, the phase-field method is a good technique as a general approach to epitaxial growth. Liu and Metiu [9] developed a phase-field model for collective motions of a train of straight steps on a crystal surface. Karma and Plappy [10] employed a phase-field model to the spiral surface growth. However, there have been no reports on applying the phase-field method to simulate nucleation and growth of islands, especially large three-dimensional islands, in epitaxy.

In this paper, we shall propose a phase-field model for nucleation and growth of islands in epitaxy. In this model, new islands nucleate spontaneously and grow at the expense of adatoms deposited randomly. By using a local phase-field variable Φ to describe different epitaxial layers of islands, the nucleation and subsequent growth of islands are formulated as a time-dependent Ginzburg-Landau-like equation coupled to a diffusive transport equation of adatoms. By employing the model for real epitaxial systems, we obtain the experimental size and spatial distributions of islands and the scaling law of the island density as a function of the ratio of the diffusion and deposition rate in the submonolayer regime. Then, through considering the asymmetric diffusion rate of adatoms on both sides of boundaries of islands, we reproduce the multilayer mounding of the metal growth systems. These simulations provide fine visualized images of the island morphologies in the submonolayer regime as well as the multilayer regime at a scale of about 100 nm. As a matter of fact, this continuum model makes the phase-field

simulation of the island growth in principle capable of covering arbitrarily large time and length scales. Moreover, the concise PDE formulation provides a natural framework to incorporate some important factors in epitaxy, especially those difficult to deal with in KMC models, such as the strain fields that occur in the presence of lattice mismatch.

In the following section we shall present our phase-field model in detail. In Sec. III we simulate island growth in the submonolayer regime. In Sec. IV, we apply the phase-field model to the growth of multilayer islands and reproduce the formation and growth of mounding structures of the metal growth systems. Finally, we conclude the paper with a summary in Sec. V.

II. PHASE-FIELD MODEL OF EPITAXIAL GROWTH

In this scheme stable islands are described by continuum variables Φ, rather than lattices as in atomic models. We take the values of Φ to be 0,1,2,3, . . . to represent in sequence the substrate, the first monolayer, the second monolayer, and so on. The sharp steps of islands used in atomic models are replaced by spatial transition zones across which Φ varies smoothly from one integer value to another. We call these transition zones phase-field transition zones (PFTZ). After being deposited on terraces, adatoms diffuse laterally with a rate D, which produces a continuum field of local adatom density. We define the diffusion rate as $D = a^2 \nu \exp(-E_d/k_B T)$, where T is the temperature, k_B is Boltzmann constant, a is the lattice constant of the physical substrates and will be taken as 1 for convenience in the following, ν is the attempt frequency, and E_d is the energy barrier of diffusion. The evolution of Φ depends on the local adatom density u.

The nucleation and growth of islands is formulated as the following differential equations:

$$\frac{\partial \Phi}{\partial t} = -\frac{1}{\tau}\frac{\delta H}{\delta \Phi} \tag{1}$$

$$= \frac{1}{\tau}[W^2 \nabla^2 \Phi - 2\sin 2\pi\Phi - \lambda u(2\cos 2\pi\Phi - 2)] + \lambda_n u^2, \tag{2}$$

$$\frac{\partial u}{\partial t} = \nabla \cdot D \nabla u - \frac{\partial \Phi}{\partial t} + \delta(r - r')\,\delta(t - t'). \tag{3}$$

Equation (1) is derived from the time-dependent Ginzburg-Landau equation constructed according to the global conservation law. H is the free energy functional defined by

$$H = \int dV \left[\frac{1}{2} W^2 (\nabla \Phi)^2 + f(\Phi, u)\right]. \tag{4}$$

The free energy density f is defined by

$$f(\Phi, u) = -\frac{1}{\pi}\cos(2\pi\Phi) + \lambda u\left(\frac{1}{\pi}\sin(2\pi\Phi) - 2\Phi\right), \tag{5}$$

in order to make H reach degenerate minimums at $\Phi = 0,1,2,3, \ldots$. The parameters W, τ, and λ are basic phase-field parameters to be determined. W represents the thickness of PFTZ, τ the characteristic time of attachment of adatoms at boundaries of islands, and λ a dimensionless coupling constant.

By using the *thin-interface analysis* we derive the expressions

$$d_0 = a_1 \frac{W}{\lambda}, \tag{6}$$

$$\beta = \frac{a_1}{\lambda}\frac{\tau}{W}\left[1 - a_2 \lambda \frac{W^2}{D\tau}\right], \tag{7}$$

which relates the phase-field parameters to the dimensionless capillarity length d_0 and the kinetic coefficient β, both of which are measurable characteristics of the system. The dimensionless capillarity length d_0 describes the deviation of the local equilibrium concentration at a curved step from that at a straight step. We know

$$d_0 = \frac{a^2 c_{eq} \gamma}{k_B T}, \tag{8}$$

where c_{eq} is the equilibrium concentration at a straight step and γ is the step stiffness. β reflects the interface kinetic in terms of $\beta = 1/\mu$, where μ is the attachment kinetic coefficient of adatoms at edges of islands. The constants a_1 and a_2 equal to 0.36 and 0.51, respectively. Here, we assume $\beta = 0$, which corresponds to fast attachment of atoms to boundaries of islands. Rearranging Eqs. (6) and (7), we obtain the following equations:

$$\lambda = \frac{a_1 W}{d_0} \tag{9}$$

and

$$\tau = \frac{a_1 a_2 W^3}{d_0 D}. \tag{10}$$

In the following we shall take W as input parameter, then determine λ and τ according to Eqs. (9) and (10).

The spatial distribution of adatoms is governed by Eq. (3). The term $\nabla \cdot D \nabla u$ describes the lateral diffusion of adatoms on the terraces. Edge diffusion is neglected for simplification, without losing main physics. The term $\partial\Phi/\partial t$ represents consumption of active adatoms due to nucleation and growth of islands. The third term on the left of Eq. (3) represents the random deposition of atoms. Whenever $t = t'$, atoms are deposited at the point of $r = r'$ with r' being determined randomly, and the adatom density u at this point is set to be 1. Here $t' = 1/(Fl^2)$, where F is the deposition rate and l is the number of the spatial grid nodes in the x (or y) direction. The random deposition of adatoms brings a sharp peak of local adatom density, which is reflected by the term $\lambda_n u^2$ in the phase-field equation so that the random deposition of atoms triggers the spontaneous nucleation of islands. The initial

nuclei are not stable, which may grow up or decay depending on the environment around themselves. The exponent 2 comes from the assumption that the critical size of an island is 1. Here we introduce a parameter λ_n to describe the nucleation rate of islands.

Adatoms on a terrace cannot climb up to upper terraces, while adatoms can go down to the lower terrace by overcoming a Schwoebel barrier E_s. In order to imitate the up-down asymmetry of adatom motion, we modify the diffusion coefficient D in PFTZ regions of island boundaries. It is identified by nonzero $|\nabla\Phi|$ in the PFTZ regions. Furthermore, according to the sign of $\nabla^2\Phi$, we divide a PFTZ region into two different parts. We change D into zero in the positive $\nabla^2\Phi$ part in order to inhibit the terrace-climbing motion of adatoms. In contrast, in the negative $\nabla^2\Phi$ part, we modify D into $D\exp(-E_s/k_BT)$ in order to imitate the effect of the Schwoebel barrier E_s on the downward motion of adatoms. With the nonconstant adatom diffusion, the phase-field model cannot be reduced exactly to the classical sharp-interface boundary conditions of the BCF model [11]. However, this is ignorable for achieving qualitative simulation results provided that the interface thickness is small.

Equations (2) and (3) are discretized in a square domain of size $l\Delta x$, where Δx is defined as the spacing of the spatial grids, by using the second-order finite differential method on uniform Cartesian grids, and by using the first-order finite differential approximation in the time domain. In addition to the restriction that $\Delta t<(\Delta x)^2/5D$, the value of time step Δt is also kept small enough to ensure the variation of Φ is less than 1 in a time step. The Neumann boundary condition is used in all directions.

III. APPLIED TO REAL GROWTH OF SUBMONOLAYER ISLANDS

In this section, we simulate the nucleation and growth of islands at the initial stage, or in the submonolayer regime, for different temperatures ranging from 293 to 529 K but a fixed flux of 0.01 monolayer per second (ML/s). We choose $E_d=0.45$ eV and $\upsilon=10^{12}$, typical values for the metal growth systems such as Fe/Fe(001). In the phase-field simulations, the growth velocity of islands is related to W. As W decreases, the growth velocity of islands increases and tends to be convergent. In practice, one must repeat computations with smaller and smaller W until the results become independent of W. Hence, W is generally chosen far less than the characteristic length of a system. In epitaxy, the characteristic length is the island separation L. Considering that L varies from several tens to several hundreds of a as the temperature increases from 293 to 529 K, we choose $W=2-10a$, which is reasonably small compared with L for the qualitative simulation.

The value of the phase-field parameter τ is related to W as well as system characteristics. The value $\beta=0$ is always assumed in the following. Assuming further that c_{eq} and γ remain constant in the whole temperature range of 293–529 K, we obtain

TABLE I. The parameters used in the phase-field simulations: temperature T (K), diffusion coefficient D (units of a^2/s), the two phase-field parameters W (units of a) and τ (s), the two simulation parameters Δx (units of a) and Δt (s), and the number of spatial grid nodes l.

T	D	W	τ	Δx	Δt	l
293	2.15×10^4	2	4.60	1	10^{-5}	350
333	1.41×10^5	3	2.70	1.5	10^{-6}	230
381	9.79×10^5	4	1.06	2	10^{-6}	180
403	2.16×10^6	4	0.50	2	10^{-6}	180
433	5.76×10^6	6	0.68	3	10^{-6}	200
483	1.83×10^7	8	1.12	4	10^{-6}	150
529	4.72×10^7	10	0.50	5	2×10^{-7}	100

$$\tau\sim\alpha\frac{W^3T}{D}, \tag{11}$$

according to which the values of τ at other temperatures can be calculated by choosing $\tau=0.5$ at $T=529$ K.

The value of λ_n should be determined in terms of the nucleation rate of islands under a certain epitaxy condition. With the case of the critical island size being set to be 1, the rate of the island nucleation is given by $(d/dt)N\sim Du^2$ according to the classical theory of the island nucleation. Associating with the classical theory of the island nucleation, we guess that λ_n must be related to D, even though there is no formulation to explicitly connect λ_n to D. Therefore, we adjust reiteratively the value of λ_n for different D at different temperatures and finally succeed in matching the simulated results to the scanning-tunneling-microscopy (STM) measurements provided in Ref. [12]. In principle, as a parameter characterizing the nucleation capability, λ_n has no relationship with the interface thickness and discretization. However, the interface thickness and discretization may influence the island nucleation just as they do the island growth in the numerical computation. We find that even with the same value of λ_n, the initial nuclei produced by the term $\lambda_n u^2$ are easier to survive and more islands are formed by using the large interface thickness and coarse discretization than by using small interface thickness and fine discretization. In the phase-field simulations, we choose reasonably small W and Δx to reduce the dependence of the simulated results on these numerical issues. The input parameters used in the simulations are summarized in Table I.

Figure 1 shows the simulated images obtained with the phase-field method. There are fewer but larger islands as the temperature increases. The morphology of these islands are consistent with the STM images of Fe/Fe(001) [12,13]. The values of λ_n are plotted in the left part of Fig. 2. It is clear that λ_n varies with D according to $\lambda_n\sim D^{0.88}$. Using these values of λ_n, we have successfully matched the simulated images to the STM ones. In the right part of Fig. 2, shown is a logarithmic plot of the density of islands versus D/F, with T varying from 293 K to 529 K, F being fixed, and a corresponding to 0.28 nm. It can be derived that the density of islands is proportional to D/F to the power of about

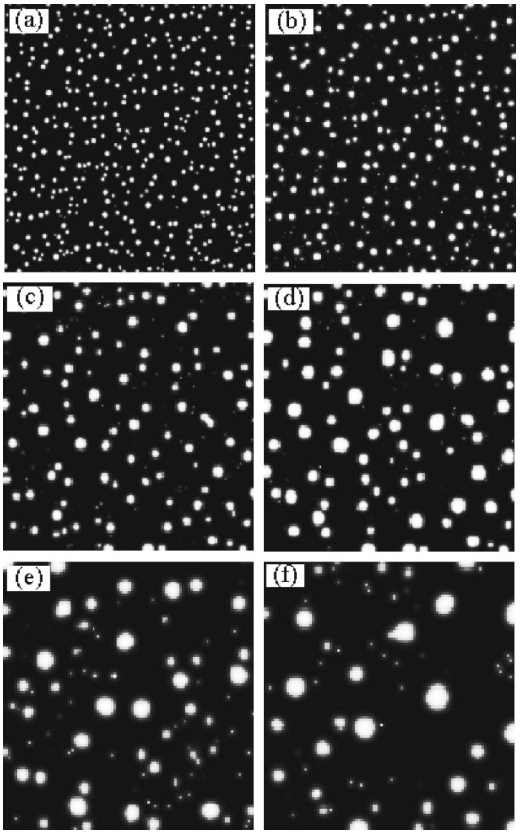

FIG. 1. The simulated images of islands on $350\times350a^2$ with the coverage of 0.07 monolayers (ML) and the flux of 0.01 ML/s at different substrate temperatures. (a) 293 K, (b) 333 K, (c) 381 K, (d) 403 K, (e) 433 K, and (f) 529 K, respectively. The phase-field and simulation parameters are the same as those in Table I.

-0.34. As is well known, for isotropic diffusion the total density of islands, N, in the low-coverage limit, varies as [12]

$$N\sim\left(\frac{D}{F}\right)^{-\chi}\exp[\chi E_d/k_BT], \tag{12}$$

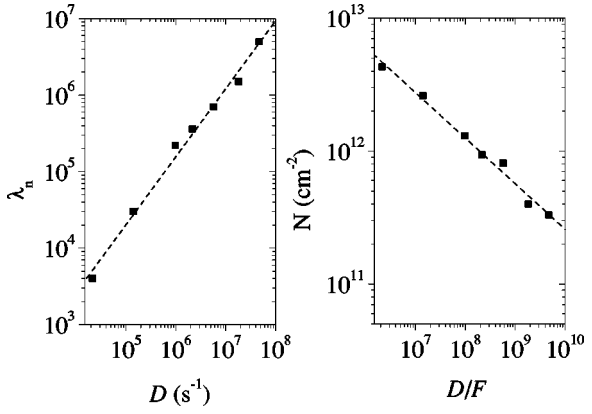

FIG. 2. The nucleation parameter λ_n vs the diffusion coefficient D (left part) and the D/F dependence of the density of islands (right part) obtained from phase-field simulations. All the parameters are the same as those in Fig. 1. The lines are the linear fits to the data.

where $\chi=i/(i+2)$. The experimental data [12,13] for Fe/Fe(001) has proved $i=1$ and $\chi=1/3$ in the temperature range of 293–529 K. Our result $\chi=0.34$ is in agreement with the experimental result.

IV. APPLIED TO REAL GROWTH OF MULTILAYER ISLANDS

The competition of growth and nucleation in the multilayer regime brings forth more multiplex morphologies. In ideal layer-by-layer growth the second-layer islands nucleate after the first layer completes. However, new stable islands (daughter islands) may nucleate on top of existing uncompleted islands (parent islands). The phenomenon is caused by the Schwoebel barrier, which resists the downward diffusion of adatoms. As a result, there appears the pyramid-like mound morphology. The mound morphology is often found in metal homoepitaxial systems with large Schwoebel barriers [14] and in metal systems even with low Schwoebel barriers but at low temperatures [15–21]. As deposition proceeds, the mounds tend to coarsen and roughen, as characterized by $L=\theta^n$ and $w=\theta^m$, respectively, where L is the mound separation and w is the roughness of the epitaxial surface.

In this section, we simulate the metal growth systems in the multilayer regime. Our strategy is to modify D on both sides of the boundaries of the islands so as to take into account the up-down asymmetry of the motion of adatoms. The downward diffusion reduced by the Schwoebel barrier E_s drives the growth into the multilayer morphology. In this way, we get the phase-field images of mounds for different deposition fluxes as shown in Fig. 3. The parameters E_s and D are set to be 0.06 eV and $800a^2/s$, respectively, which correspond to the island growth of metal systems with immediate Schwoebel barriers at low temperature. The mounds become larger with the height increasing from 2 to 5 atomic layers as the deposition flux decreases. The highest layer is located at the tops of the mounds, and the lowest layers are connected, forming channels at the bases. The mound morphologies as shown in Fig. 3 resemble those that have been observed in some typical metal systems, for example, Fe(001) [15] and Ag(100) [16]. Figure 4 presents the snapshots of the epitaxial growth in the simulation for $F=0.02$ ML/s at different coverages, which reveals coarsening and roughening of the mounds.

In order to characterize the mounding behavior, we examined the height-height correlation function of the morphology, $H(r)$, i.e., the mean-square height difference for two points of the substrate versus their lateral separation r. In terms of $H(r)$, we get the roughness w of the epitaxial islands, $\sqrt{\langle H(0)H(0)\rangle}$, and the mound separation $L=2r_c$, where r_c is the position of the first zero crossing of $\langle H(r)H(0)\rangle$. The results are plotted in Figs. 5 and 6. The inset in Fig. 5 shows $H(r)$ versus r for $F=0.02$ ML/s.

As for coarsening of the mounds, the experimental data of the coarsening exponent n in the low temperature regimes is about 0.16 ± 0.04 for Fe(001) at 293 K [15], 0.20 ± 0.02 for Ag(100) at 190–260 K [17], and 0.25–0.50 for Cu(100) at 160–200 K [18]. A continuum model without capillarity predicts $n\sim1/6$ [15], whereas the theoretical works [19,20] in-

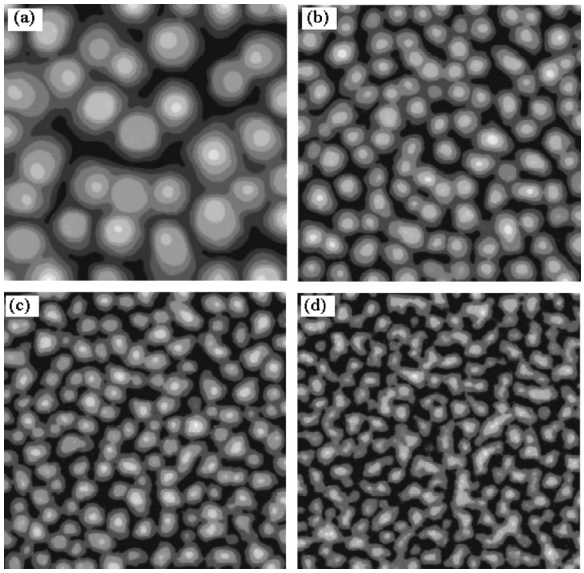

FIG. 3. The simulated morphology of $300\times300a^2$ at $\theta=6$ monolayers (ML), for (a) $F=0.001$ ML/s, (b) $F=0.01$ ML/s, (c) $F=0.02$ ML/s, and (d) $F=0.05$ ML/s by using $W=2$ and $\tau=1$. The diffusion barrier is 0.45 eV and the temperature is 250 K. The absolute heights of the highest islands in (a), (b), (c), and (d) are 12, 9, 9, and 7 atomic layers (AL), respectively, but their relative heights with respect to the deepest valleys are 7, 5, 4, and 2 AL, respectively.

cluding capillary-induced mound coalescence predict $n=0.25$. These experimental and theoretical results indicate that capillarity induces coalescence of mounds, driving mounds to coarsen faster than they do in the case of zero or

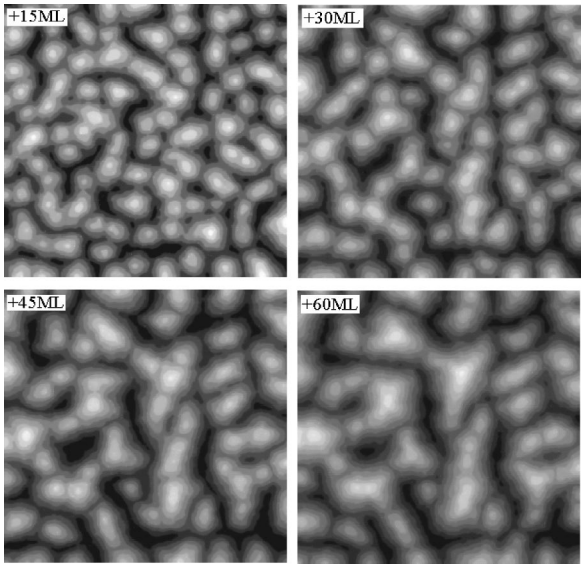

FIG. 4. The simulated morphology of $300\times300a^2$ for different coverages: 15, 30, 45, and 60 monolayers (ML) (upper-left to lower-right panel) with $F=0.02$ ML/s by using $W=2$ and $\tau=1$. The diffusion barrier is 0.45 eV and the temperature is 250 K. The absolute heights of the highest islands are 18, 33, 52, and 68 atomic layers (AL), respectively, but their relative heights with respect to the deepest valleys are 7, 8, 10, and 11 AL, respectively.

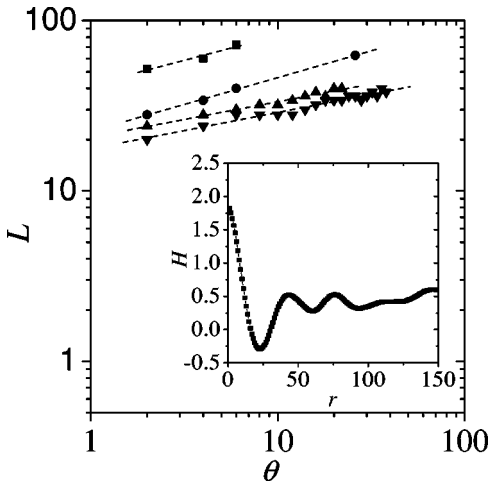

FIG. 5. The simulated results for average mound separation L (units of a) vs coverage θ [units of monolayer (ML)] for flux F of 0.001, 0.01, 0.02, and 0.05 ML/s (top to bottom). Other parameters are the same as those in Figs. 3 and 4. Inset: The height-height correlation function H (units of a) as a function of lateral distance r (units of a) at $F=0.02$ ML/s.

weak capillarity. Our phase-field model is based on the BCF model including capillarity, hence coalescence induced by capillarity is an apparent feature in our simulations, as shown in Fig. 4. The linear fit in Fig. 5 indicates that the mounds in our simulation grow with a coarsening exponent of 0.25 ± 0.05, being larger than those for Fe (001) and Ag (100), where no substantial coalescence of mounds occurs, but consistent with the theoretical prediction including capillary-induced mound coalescence.

The roughening exponent m varies with the specific systems in a larger range than the coarsening exponent does. It was shown experimentally that m is about 0.18 for Fe(001) [21], 0.40 for Ag(100) [16], and 0.25–0.50 for Cu(100) [18]. The theoretical prediction is that $m=n=0.25$ [19]. In our simulations, $m=0.30\pm0.01$ as indicated in Fig. 6, which is

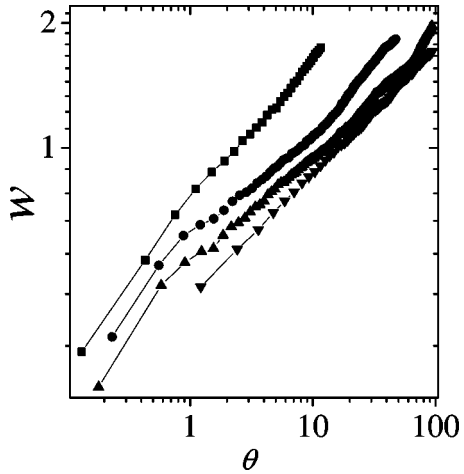

FIG. 6. The simulated results for roughness w vs coverage θ [units of monolayer (ML)] for fluxes of 0.001, 0.01, 0.02, and 0.05 ML/s (top to bottom). Other parameters are the same as those in Figs. 3 and 4.

reasonable compared with the above experimental and theoretical data. As is generally observed, m is a little larger than n in our simulations, indicating roughening is more rapid than coarsening during the development of mounds. Furthermore, the obtained m and n is close to a quarter for different fluxes ranging from 0.001 to 0.05 ML/s, indicating that the deposition flux has no effective influence on the coarsening and roughening of mounds.

V. CONCLUSION

In summary, we have proposed a phase-field method to model the epitaxial growth of adatom islands. By using the model, we obtain the experimental local size and shape of islands and the well known scaling law of the island density, $N \sim D/F^{-\chi}$ with $\chi = 0.34$, in the submonolayer regime. By modifying diffusion coefficient D around the step regions, we reproduce the mounding structure with the coarsening exponent of 0.25 ± 0.05 and roughening exponent of 0.30 ± 0.01 in the multilayer regime for the metal growth systems. The simulations in this paper are conducted on the length scales of about 100 nm and time scales of several tens to thousands of seconds. With optimized parameters, the phase-field simulation can reach much larger scales. Therefore, the phase-field model is a good approach advantageous over atomic models and analytic mean-field models for simulating the adatom island growth in epitaxy on a large scale of practical engineering interests. Moreover, the concise formulation and easy numerical resolution makes it easy to incorporate into the phase-field model various relevant information from atomic models. It is also easy to couple the phase field with other physical fields so that some hybrid models that can deal with more complex epitaxial processes will be constructed.

ACKNOWLEDGMENTS

This work was supported by the Chinese Department of Science and Technology under the National Basic Research Projects (Project No. G1999064509), and by the Nature Science Foundation of China (Grant Nos. 60021403 and 10134030).

[1] W.K. Burton, N. Cabrera, and F.C. Frank, Philos. Trans. R. Soc. London, Ser. A **243**, 299 (1951).
[2] M.F. Gyure, C. Ratsch, B. Merriman, R.E. Caflisch, S. Osher, J.J. Zinck, and D.D. Vvedensky, Phys. Rev. E **58**, R6927 (1998); C. Ratsch, M.F. Gyure, R.E. Caflisch, F. Gibou, M. Petersen, M. Kang, J. Garcia, and D.D. Vvedensky, Phys. Rev. B **65**, 195403 (2002); C. Ratsch, M. Kang, and R.E. Caflisch, Phys. Rev. E **64**, 020601 (2001); F.G. Gibou, C. Ratsch, M.F. Gyure, S. Chen, and R.E. Caflisch, Phys. Rev. B **63**, 115401 (2001).
[3] D.L. Chopp, J. Comput. Phys. **162**, 104 (2000).
[4] R. Kobayashi, Physica D **63**, 410 (1993); N.A. Ahmad, A.A. Wheeler, W.J. Boettinger, and G.B. McFadden, Phys. Rev. E **58**, 3436 (1998); A. Karma, Phys. Rev. Lett. **87**, 115701 (2001); R. Folch and M. Plapp, Phys. Rev. E **68**, 010602 (2003); B. Nestler, A.A. Wheeler, L. Ratke, and C. Stacker, Physica D **141**, 133 (2000); A.M. Mullis, Phys. Rev. E **68**, 011602 (2003).
[5] A.E. Lobkovsky and J.A. Warren, Phys. Rev. E **63**, 051605 (2001).
[6] M. Conti, B. Meerson, A. Peleg, and P.V. Sasorov, Phys. Rev. E **65**, 046117 (2002).
[7] L. Granasy, T. Borzsonyi, and T. Pusztai, Phys. Rev. Lett. **88**, 206105 (2002); M. Castro, Phys. Rev. B **67**, 035412 (2003).
[8] A. Karma and W.-J. Rappel, Phys. Rev. Lett. **77**, 4050 (1996).
[9] F. Liu and H. Metiu, Phys. Rev. E **49**, 2601 (1994).
[10] A. Karma and M. Plapp, Phys. Rev. Lett. **81**, 4444 (1998).
[11] O. Pierre-Louis, Phys. Rev. E **68**, 021604 (2003).
[12] J.A. Stroscio and D.T. Pierce, Phys. Rev. B **49**, 8522 (1994).
[13] J.A. Stroscio, D.T. Pierce, and R.A. Dragoset, Phys. Rev. Lett. **70**, 3615 (1993).
[14] W.C. Elliott, P.F. Miceli, T. Tse, and P.W. Stephens, Phys. Rev. B **54**, 17 938 (1996); F. Tsui, J. Wellman, C. Uher, and R. Clarke, Phys. Rev. Lett. **76**, 3164 (1996); M. Kalff, P. Smilauer, G. Comsa, and T. Michely, Surf. Sci. **426**, L447 (1999).
[15] J.A. Stroscio, D.T. Pierce, M.D. Stiles, A. Zangwill, and L.M. Sander, Phys. Rev. Lett. **75**, 4246 (1995).
[16] K.J. Caspersen, A.R. Layson, C.R. Stoldt, V. Fournee, P.A. Thiel, and J.W. Evans, Phys. Rev. B **65**, 193407 (2002).
[17] C.R. Stoldt, K.J. Caspersen, M.C. Bartelt, C.J. Jenks, J.W. Evans, and P.A. Thiel, Phys. Rev. Lett. **85**, 800 (2000).
[18] H.J. Ernst, F. Fabre, R. Folkerts, and J. Lapujoulade, Phys. Rev. Lett. **72**, 112 (1994); J.-K. Zuo and J.F. Wendelken, *ibid.* **78**, 2791 (1997).
[19] A.W. Hunt, C. Orme, D.R.M. Williams, B.G. Orr, and L.M. Sander, Europhys. Lett. **27**, 611 (1994).
[20] M. Siegert and M. Plischke, Phys. Rev. Lett. **73**, 1517 (1994).
[21] M.C. Bartelt, and J.W. Evans, Phys. Rev. Lett. **75**, 4250 (1995).